INSTITUTE OF PHYSICS PUBLISHING JOURNAL OF PHYSICS B: ATOMIC, MOLECULAR AND OPTICAL PHYSICS

J. Phys. B: At. Mol. Opt. Phys. **36** (2003) 4717–4729 PII: S0953-4075(03)67367-0

CH_4 ionization and dissociation by proton and electron impact

H Luna[1], E G Cavalcanti[1], J Nickles[1,2], G M Sigaud[1] and E C Montenegro[1,3]

[1] Departamento de Física, Pontifícia Universidade Católica do Rio de Janeiro, Caixa Postal 38071, Rio de Janeiro, RJ 22452-970, Brazil
[2] Institut für Kernphysik, August-Euler-Strasse 6, D-60486, Frankfurt am Main, Germany

E-mail: ecmo@vdg.fis.puc-rio.br

Received 6 August 2003
Published 11 November 2003
Online at stacks.iop.org/JPhysB/36/4717

Abstract

Absolute dissociative and non-dissociative ionization cross sections of CH_n^+ ($n = 0$–4) molecules by protons in the 0.5–3.5 MeV impact energy range have been measured. The present results are in good agreement with the previously published data, where overlap occurs. A decay-route model for CH_4 dissociation induced by proton impact is proposed and a method to obtain the corresponding branching ratios is introduced. The consistency and extent of the proposed model and methodology is verified through its application in the case of electron-impact dissociation.

1. Introduction

Interest in molecules present in interplanetary atmospheres and cometary gases has increased in recent years because of new discoveries in the space research programme. One example is Titan's atmosphere [1], composed of 97% N_2, the remainder being CH_4 and other hydrocarbons. Because of this composition, Titan's atmosphere is often thought to resemble the primordial atmosphere on Earth. The dissociation of CH_4 by UV photons, electrons and cosmic rays produces highly reactive radicals which not only combine to form more complex molecules [2] but also contribute to significantly change the methane concentration in the upper atmosphere of Titan, due to chemical coupling between ionic and neutral species [3]. These new developments have made it necessary to have accurate measurements concerning absolute cross sections for ionization, electron capture and dissociation processes as well as the energy and momentum distribution of molecular fragments created through the interaction with electrons, ions and photons. These cross sections are also needed for atmospheric

[3] Author to whom any correspondence should be addressed.

0953-4075/03/234717+13$30.00

plasma calculations involving heating processes, collisional ejection of atoms and molecules (atmospheric sputtering) and expansion of the corona [4, 5].

Methane is also the simplest hydrocarbon used for the preparation of diamond and diamond-like materials [6]. Very hard diamond-like carbon films are grown by dissociating methane in an RF discharge of electron cyclotron resonance reactors [7]. The modelling of these processes requires the inclusion of a large number of dissociated species and chemical reactions [7] which are mainly driven by electron impact.

In the above-mentioned applications not only the absolute cross sections but also the branching ratios for the various dissociation paths of methane induced by charged particles are needed. In the last years some work has been done concerning the interaction of CH_4 with ions, electrons and photons. In the case of protons, Browning and Gilbody [8] have measured CH_4 molecule ionization and dissociation induced by 5–50 keV protons. Their data were normalized to the cross section for total ion production measured by Carré [9] at 30 keV. Malhi *et al* [10] measured the single charged molecular ion cross sections, CH_n^+ ($n = 0$–4) from a CH_4 target, for high-energy protons. This measurement was performed in the energy range of 1–11 MeV and a magnetic spectrometer was used to select the target products by mass/charge. The molecular ion production cross sections were normalized to the Ne ion production cross section by F^{9+} ions incident at 1 MeV amu^{-1} measured by Gray *et al* [11].

Later, Ben-Itzhak *et al* [12, 13] performed, in the same energy range (1–12 MeV), detailed product-discriminated experiments for protons impinging on CH_4. In those experiments they were able to measure the relative yield of single ion, ion-pair and ion-triple channels production using a coincidence time-of-flight technique. Total multiple-ionization cross sections were obtained by normalizing the measured yields to the CH_4^+ production cross sections from Malhi *et al* [10]. By the same time, in another set of measurements, Knudsen *et al* [14] had obtained the single-ion production cross sections for CH_n^+ ($n = 1$–4), C^+, H_2^+ and H^+ target products for proton and antiproton impact over the energy range of 50 keV–6 MeV. Their proton data were normalized at 2 MeV to their previous positron data at the same velocity [15].

Although there are also several measurements for electron-impact dissociative ionization of methane [16–18], the use of these experimental data to make a comprehensive decay scheme for both electron and proton impact covering a broad range of projectile velocities was not, to the authors' knowledge, carried out. The main difficulty in obtaining such a scheme comes from the double-ionization contribution, which plays an important role in the formation of highly dissociated products such as CH^+ and C^+. Double ionization can be reached either by two-step ionization or by several different autoionization mechanisms which depend critically on the energy transferred to the CH_4, as shown by several studies of dissociative photoionization [19–22].

The purpose of this work is two-fold. First, to provide independent absolute cross sections for total single-ion production of a CH_4 target, namely CH_n^+ ($n = 0$–4), in collisions with 0.5–3.5 MeV protons. Our data fill the gap left by the measurements of Knudsen *et al* [14] and Ben-Itzhak *et al* [12, 13], between 460 keV and 1 MeV. Second, to propose a decay-route model for CH_4 which includes both single and double ionization and from which all the branching ratios can be obtained from the available experimental data. The model is then applied to electron-impact dissociation to check its consistency and extent.

2. Experiment

The experimental set-up used in this work was described in a previous paper [23], except for some minor modifications concerning the projectile detecting system described by Cavalcanti *et al* [24].

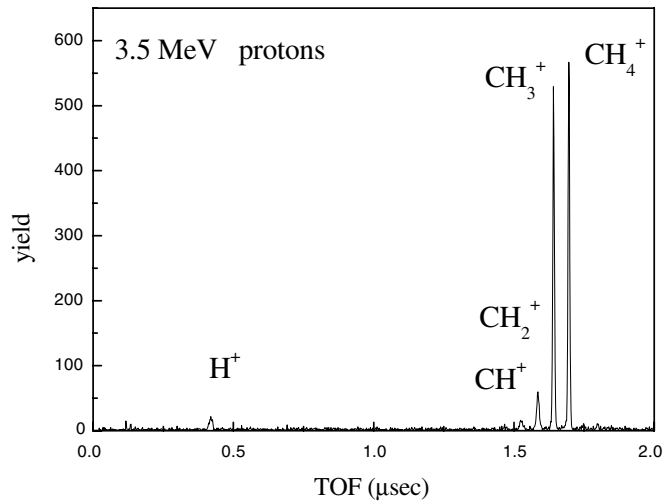

Figure 1. Typical time-of-flight spectrum of CH_4 for 3.5 MeV proton impact.

In short, collimated monoenergetic proton beams, with energies ranging from 0.5 to 3.5 MeV, are delivered by the 4 MV van de Graaff accelerator of the Catholic University of Rio de Janeiro. The selection of the charge, mass and energy of the beam is made by a 90° magnet followed by a switching magnet before the entrance of the beam line. A third magnet just before the collision chamber cleans the main beam of spurious components. The projectile beam then crosses a target cell, eventually producing ions by collision with the CH_4 target gas. A capacitive manometer measures the absolute pressure inside the target cell, with a typical operating pressure of 0.5 mTorr. This pressure ensures a single-collision regime. After leaving the target cell, the emergent beam is analysed by a fourth magnet and directed onto a microchannel plate detector placed at the end of the beam line. A 600 Å thick Al diffuser placed 4 m upstream of the projectile detector is used to guarantee a broad illumination over the entire sensitive area of the detector. This set-up allowed us to work with projectile counting rates up to 30 k/s without having any significant loss of detector efficiency.

The ions formed from the target are collected by a transverse electric field. The use of a strong field (500 V cm^{-1}) ensures the maximum collecting efficiency for all target products except for the H^+ ions. These ions have a large dissociation speed as they carry a large part of the dissociation energy, of the order of few eV. During the extraction process some of these ions are lost. Our H^+/CH_4^+ ratio is about 5% in average, which is roughly a factor of 2 smaller than that obtained by Ben-Itzhak *et al* [12, 13]. A highly transparent grid permits the target products to pass the electrodes, enter a field-free region and, finally, go on to a microchannel plate detector. These various dissociative and non-dissociative target products were separated according to their charge/mass ratio using a standard time-of-flight technique. A small delay was used to set the proton peak out of the start–stop coincidence. This is necessary to avoid the loss of double-ionization channels involving H^+ production: $H^+ + CH_3^+$, $H^+ + CH_2^+$, $H^+ + CH^+$ and $H^+ + C^+$. A typical time-of-flight spectrum for 3.5 MeV is shown in figure 1.

Our absolute cross sections for CH_n^+ ($n = 0$–4) production are presented in table 1. Figures 2–6 show our absolute cross sections (full circles) together with the experimental data reported by Browning and Gilbody [8] (asterisks), Knudsen *et al* [14] (open triangles), and Ben-Itzhak *et al* [13] (open squares). The carbon K-shell ion (crosses) is also plotted in figure 6 [25, 26] (see also [27]) to indicate the magnitude of that contribution. The single-hole

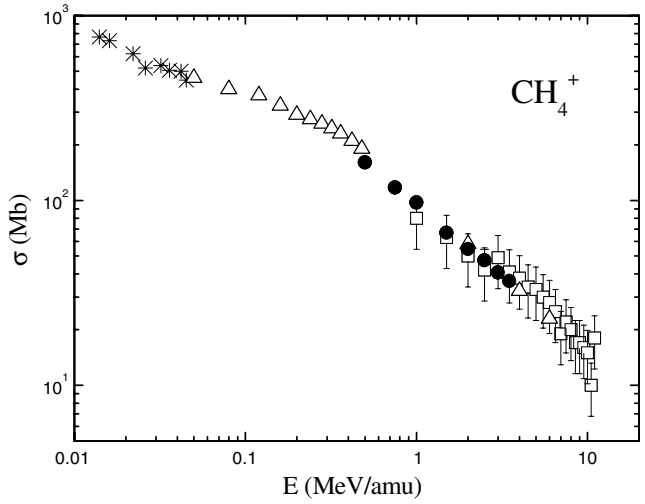

Figure 2. Absolute cross sections for CH_4^+ production: ●, this work; ∗, [8]; △, [14]; □, [13].

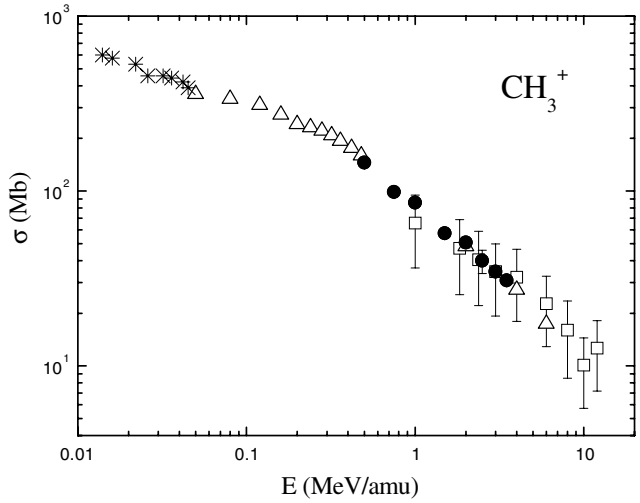

Figure 3. Absolute cross sections for CH_3^+ production: ●, this work; ∗, [8]; △, [14]; □, [13].

fluorescence yields of Krause [28] were used to convert the K-shell x-ray production into the K-shell ionization cross section. Overall, our measurements are in very good agreement, where the data overlap, with those of Knudsen *et al* [14] and Ben-Itzhak *et al* [13] for all dissociation products. Considering that the absolute values presented in figures 2–6 are independently obtained, they can be considered reliable enough to construct a dynamical model for the CH_4 decay as described in the following sections.

3. Dynamical decay routes of CH_4

Experiments on photoionization of CH_4 [19–22] have shown that the large variety of dissociation products which are observed are markedly dependent on the energy transferred to

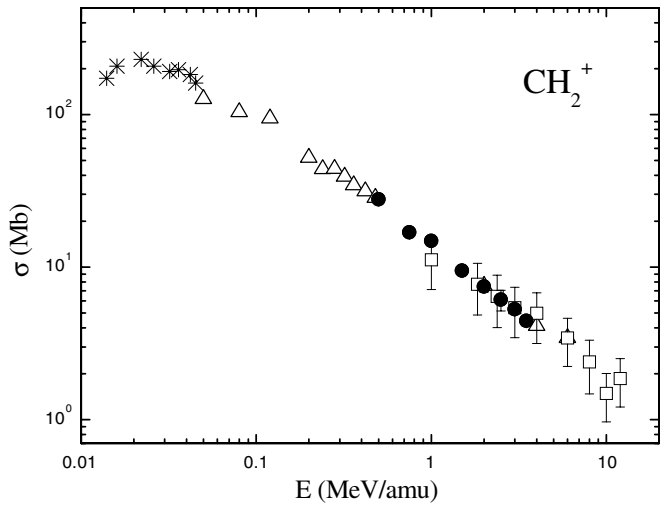

Figure 4. Absolute cross sections for CH_2^+ production: ●, this work; ∗, [8]; △, [14]; □, [13].

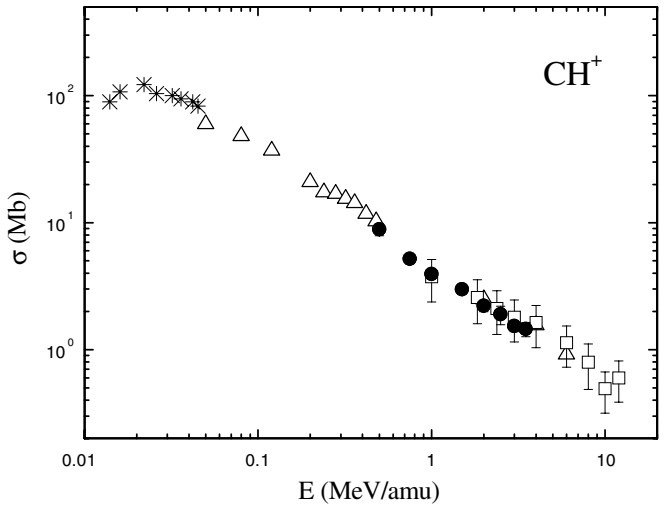

Figure 5. Absolute cross sections for CH^+ production: ●, this work; ∗, [8]; △, [14]; □, [13].

the molecule. In the case of charged particle impact, the energy transfer is not well defined in experiments which measure only the dissociation products, and the sharp features governing dissociation, which appear in the photon case, are smeared out. As experiments giving detailed information on the energy transfer induced by charged particles are very scarce [16], and theoretical calculations are essentially non-existent, the building of a decay route of the CH_4 five-body decay can only be done in a limited way, using some general features taken from the photon case.

Although constrained by the above-mentioned remarks, it is possible to design a decay scheme, as shown in figure 7, which can fit the charged particle data quite well. The main assumption of the model is to consider three sequential routes coming from two independent primary sources—single ionization or double ionization. Each sequential route is characterized

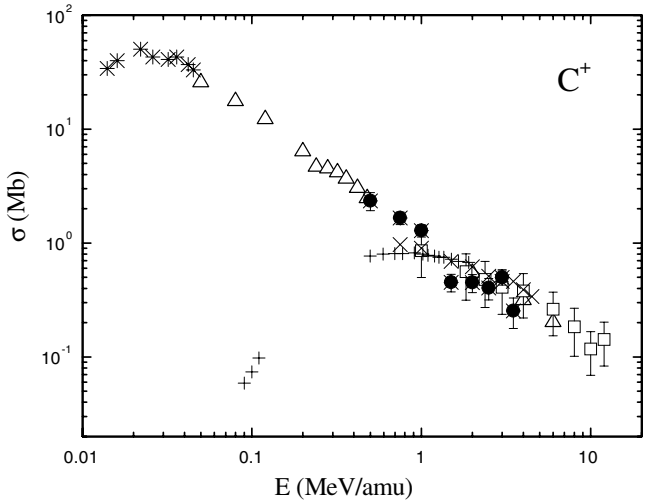

Figure 6. Absolute cross sections for C^+ production: ●, this work; ∗, [8]; △, [14]; □, [13]; +, [25]; ×, [26].

Table 1. Absolute multiple-ionization cross sections of CH_4 by protons (Mb).

E (MeV)	CH_4^+	CH_3^+	CH_2^+	CH^+	C^+
0.50	160 ± 9	145 ± 8	27.8 ± 2	8.84 ± 0.95	2.35 ± 0.42
0.75	117 ± 5	98.5 ± 4.5	16.9 ± 1	5.17 ± 0.41	1.66 ± 0.21
1.00	97.0 ± 2.3	85.5 ± 2	14.8 ± 0.6	3.93 ± 0.28	1.28 ± 0.16
1.50	66.6 ± 3.7	57.1 ± 3.1	9.44 ± 0.61	2.97 ± 0.25	0.45 ± 0.08
2.00	54.4 ± 3.5	50.8 ± 3.2	7.43 ± 0.55	2.20 ± 0.22	0.45 ± 0.08
2.50	47.2 ± 7.1	39.8 ± 6	6.11 ± 0.94	1.88 ± 0.31	0.40 ± 0.09
3.00	40.6 ± 2.5	34.5 ± 2.1	5.28 ± 0.38	1.53 ± 0.14	0.49 ± 0.07
3.50	36.6 ± 1.4	30.8 ± 1.2	4.44 ± 0.34	1.45 ± 0.18	0.25 ± 0.08

by *stabilization probabilities*, which are the probabilities of molecular excited states stabilizing into the ground state. For example, p_1 is the probability of the CH^{+*} ion, which results from the decay of the parent CH_2^{+*} ion, both in excited states, stabilizing in CH^+. If the CH^{+*} does not stabilize in CH^+, it must decay into C^+ with a probability $1 - p_1$. It can be seen that a possible alternative branch, giving C^0 plus H^+, is not considered. This as well as some other energetically possible branches are assumed negligible by the model shown in figure 7. This assumption relies on the fact that the final state for this last route has a larger energy than the former [19] and ionization by swift charged particles preferentially favour small energy transfers.

Route I in figure 7 is associated with soft collisions. Indeed, the stable CH_4^+ ion is never observed if CH_4 is excited above 15 eV [19, 29]. The configuration of CH_4 is $(1a_1)^2(2a_1)^2(1t_2)^6$ where $1a_1$ and $2a_1$ correspond to the 1s and 2s orbitals respectively of the carbon atom, with the two valence states of the ion being the so-called $X(1t_2)^{-1}$ ground state and the $A(2a_1)^{-1}$ excited state [22]. If the CH_4^{+*} does not stabilize as CH_4^+, the excited molecule follows a sequential path until it reaches a stable configuration. Another branch indicated as coming from the excited CH_4^{+*}, shown in figure 7, is the decay to $CH_3^0 + H^+$. The H^+ production has a threshold at 21.6 eV [22]. Because this threshold energy is below the $(2a_1)^{-1}$ threshold, which occurs at 22.4 eV, some of the H^+ produced might come from autoionizing Rydberg

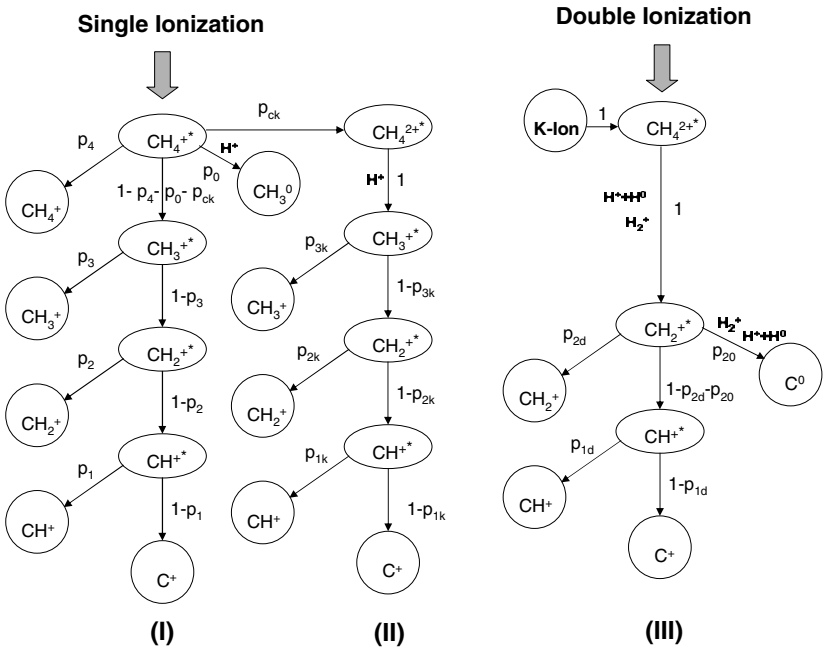

Figure 7. Decay-scheme diagram for CH_4 dissociation induced by charged particles.

states ($2a_1^{-1}3pt_2$ or $2a_1^{-1}4pt_2$) of CH_4^{0*} as pointed out by Latimer *et al* [22] and Mathur [30]. This possibility can be considered as implicitly included in the probability p_0, although not explicitly indicated in figure 7.

Following Furuya *et al* [29], the major processes for CH_3^+ production are: (i) through vibrationally excited $(1t_2)^{-1}$ ionic states located above 14.3 eV; (ii) through autoionization from low-Rydberg states $2a_1^{-1}3pt_2$ or $2a_1^{-1}4pt_2$ (see also [22]). The first process is considered in route I of figure 7. The second process gives rise to route II of figure 7 to which a probability p_{ck} is associated. Within the simplifications of the present model these are the only two pathways in which CH_3^+ is formed, both of them originating from the single-ionization process. This is in agreement with the observed fact (see later) that the ratio CH_3^+/CH_4^+ is pretty much independent of the projectile velocity, for any measured velocity. Because the energy transfers by the projectile in these two routes are rather similar, we assumed that $p_{3k} = p_3$, $p_{2k} = p_2$ and $p_{1k} = p_1$ in the forthcoming analysis.

Route III in figure 7 is associated with doubly ionized CH_4^{2+}. As stable CH_4^{2+} has never been observed in mass spectrometry induced by charged-particle impact [12, 16, 31, 32], this decay route must involve the emission of one or more hydrogen nuclei. As observed above, the CH_3^+/CH_4^+ ratio is independent of the projectile velocity (see also [12]). Because CH_4^+ production is essentially due to single ionization, the same must happen with CH_3^+. Some post-collisional decay following single ionization can eventually occur, as indicated in route II of figure 7, but no substantial CH_3^+ production is apparently associated with primary double ionization. Indeed, the presence of this mechanism would be reflected by an observable dependence of the CH_3^+/CH_4^+ ratio on the projectile velocity, which has not been seen. In double-photoionization experiments the most abundant decay channels give $H^+ + CH_3^+$, $H^+ + CH_2^+$ and $H_2^+ + CH_2^+$ as possible primary charged products of the reaction. However, the $CH_4^{2+*} \rightarrow H^+ + CH_3^+$ dissociation channel is important only near the double-photoionization

threshold, around 35 eV [31]. For photon energies above 38.5 eV the more likely dissociation channel is $CH_4^{2+*} \rightarrow H^+ + H^0 + CH_2^+$ [31]. As the double-photoionization cross section rises sharply with the energy transferred, until reaching the maximum value around 47 eV, it is possible that the dynamics of double ionization by charged particles weighs the various possible energy transfers which contributes to the double ionization in such a way that the $CH_4^{2+*} \rightarrow H^+ + H^0 + CH_2^+$ channel dominates. The identification of this channel as the main fragmentation product associated with double ionization has been reported in both electron-impact [16] and proton-impact experiments [12]. According to this scenario, figure 7 assumes that CH_4^{2+*} decays into a CH_2^{+*} excited state which, in turn, might result in either a stabilization of CH_2^+, or a further decay to C^0 or CH^{+*}. Other decay modes not included in figure 7, such as $CH_2^{+*} \rightarrow H^0 + H^0 + C^+$, are possible, but as they involve larger internal energies [31] they were neglected in the present, simplified model. As the CH_4^{2+*} production through carbon K-shell ionization followed by Auger emission also involves a large energy transfer to the molecule, this production mechanism was included as an alternative source of this route, denoted in figure 7 as K-ion.

4. Determination of the stabilization probabilities

According to figure 7, and denoting by σ_I, σ_{DI} and σ_K the cross sections for single, double and carbon K-shell ionization, respectively, the cross sections for CH_n^+ ($n = 0$–4) production are given by

$$\sigma_{CH_4^+} = p_4\sigma_I, \tag{1}$$

$$\sigma_{CH_3^+} = [p_3(1 - p_4 - p_0 - p_{ck}) + p_{3k}p_{ck}]\sigma_I, \tag{2}$$

$$\sigma_{CH_2^+} = [p_2(1 - p_3)(1 - p_4 - p_0 - p_{ck}) + p_{2k}(1 - p_{3k})p_{ck}]\sigma_I + p_{2d}(\sigma_{DI} + \sigma_K), \tag{3}$$

$$\sigma_{CH^+} = [p_1(1 - p_2)(1 - p_3)(1 - p_4 - p_0 - p_{ck}) + p_{1k}(1 - p_{2k})(1 - p_{3k})p_{ck}]\sigma_I + p_{1d}(1 - p_{2d} - p_{20})(\sigma_{DI} + \sigma_K), \tag{4}$$

$$\sigma_{C^+} = [(1 - p_1)(1 - p_2)(1 - p_3)(1 - p_4 - p_0 - p_{ck}) + (1 - p_{1k})(1 - p_{2k}) \times (1 - p_{3k})p_{ck}]\sigma_I + (1 - p_{1d})(1 - p_{2d} - p_{20})(\sigma_{DI} + \sigma_K), \tag{5}$$

which gives the following ratios relative to CH_4^+

$$R_{34} = \frac{p_3(1 - p_4 - p_0 - p_{ck}) + p_{3k}p_{ck}}{p_4}, \tag{6}$$

$$R_{24} = \frac{p_2(1 - p_3)(1 - p_4 - p_0 - p_{ck}) + p_{2k}(1 - p_{3k})p_{ck}}{p_4} + p_{2d}\left(\frac{\sigma_{DI} + \sigma_K}{\sigma_{CH_4^+}}\right), \tag{7}$$

$$R_{14} = \frac{p_1(1 - p_2)(1 - p_3)(1 - p_4 - p_0 - p_{ck}) + p_{1k}(1 - p_{2k})(1 - p_{3k})p_{ck}}{p_4} + p_{1d}(1 - p_{2d} - p_{20})\left(\frac{\sigma_{DI} + \sigma_K}{\sigma_{CH_4^+}}\right), \tag{8}$$

$$R_{04} = \frac{(1 - p_1)(1 - p_2)(1 - p_3)(1 - p_4 - p_0 - p_{ck}) + (1 - p_{1k})(1 - p_{2k})(1 - p_{3k})p_{ck}}{p_4} + (1 - p_{1d})(1 - p_{2d} - p_{20})\left(\frac{\sigma_{DI} + \sigma_K}{\sigma_{CH_4^+}}\right). \tag{9}$$

Equations (6)–(9) are linear functions of the ratios $(\sigma_{DI} + \sigma_K)/\sigma_{CH_4^+}$, and can be used to obtain the model parameters. Indeed, eight conditions involving these parameters can be straightforwardly obtained from the intercept and slope of these four equations. Assuming

$p_{3k} = p_3$, $p_{2k} = p_2$, and $p_{1k} = p_1$, as discussed before, the nine stabilization probabilities left can be obtained by least-square linear fits to the above ratios with some additional information on the H^+ plus H_2^+ production.

To this end, an estimate of σ_K and σ_{DI} cross sections is needed. The carbon K-shell ionization cross sections are well known and were taken from [25–27]. The main difficulty lies in having a reliable estimate of the methane double-ionization cross section, by protons, over a wide range of velocities. To the authors' knowledge, there are no experiments or theoretical calculations reported for this case. In fact, the use of experimental results to obtain double-ionization cross sections can be masked by the contribution of autoionization at intermediate to high velocities, as clearly shown by Cavalcanti *et al* [24] for the case of Ne.

The simplest procedure for estimating the double-ionization cross section is to take advantage of the well-known Born result, as discussed by Sant'Anna *et al* [33]. At high velocities, the cross sections are quite insensitive to the details of the wavefunctions of the active electrons and depend, mainly, on the ionization energies. This result gives rise to simple scaling laws expressing the cross sections of one system in terms of another. Single- and double-ionization cross sections of Ne, which is isoelectronic to CH_4, have been recently calculated by Kirchner *et al* [34] using the independent particle model. According to the scaling laws described in [33], the double-to-single ionization ratios, $R_{DS}(E) = \sigma_{DI}(E)/\sigma_{SI}(E)$ for CH_4 and Ne, as a function of the projectile energy E, are related as

$$[R_{DS}(E)]_{CH_4} = A\alpha[R_{DS}(\alpha E)]_{Ne}, \tag{10}$$

where $\alpha = (2/I_{2a_1}+6/I_{1t_2})/(2/I_{2s}+6/I_{2p})$ and $I_{2a_1} = 22.4\,\text{eV}$, $I_{1t_2} = 12.6\,\text{eV}$, $I_{2s} = 40.96\,\text{eV}$ and $I_{2p} = 21.56$ eV are the ionization energies of the outermost shells of CH_4 and Ne respectively (see [33]). In a previous work [24] it was found that the calculations of [34] agree quite well, in shape, with the measured double ionization of Ne. However, the absolute values overestimate the experiment by a factor of nearly 2. The constant A in the above equation takes this discrepancy into account, and was taken as $A = 1/2$, i.e. the same as in the case of Ne. For proton energies 5 keV $< E <$ 5000 keV, the ratio $[R_{DS}]_{Ne}$ can be approximated, within 5%, by $[R_{DS}]_{Ne} = 0.0006E^{2.2}/(1 + 0.03E)^{3.2}$ with E given in keV.

Using measured values of $\sigma_{CH_4^+}$ as well as σ_K and σ_{DI} determined as described above, the ratios R_{n4} (n = 0–3) can be plotted as a function of $(\sigma_{DI} + \sigma_K)/\sigma_{CH_4^+}$. This is shown in figures 8(a)–(d). The lines are best linear fits to the data and the stabilization probabilities were chosen to give straight lines which overlap with them. This procedure gives: $p_4 = 0.49$, $p_3 = 0.84$, $p_2 = 0.75$, $p_1 = 0.87$, $p_{ck} = 0.012$, $p_0 = 0.03$, $p_{2d} = 0.48$, $p_{1d} = 0.68$, and $p_{20} = 0.12$. A fine adjustment, mainly regarding the probability p_{ck}, was carried out comparing the H^+ plus H_2^+ production cross section as given by the present model (see figure 7),

$$\sigma_{H^+ + H_2^+} = (p_{ck} + p_0)\sigma_I + (1 + p_{20})(\sigma_{DI} + \sigma_K), \tag{11}$$

with those reported by Ben-Itzhak *et al* [13]. Figure 9 shows the cross sections $\sigma_{H^+ + H_2^+}$ determined through equation (11) compared with the proton measurements by Ben-Itzhak *et al* [13] and the equivelocity electron measurements by Straub *et al* [17] and Cechan and Vidal [18]. The agreement among all measurements and the calculations from equation (11) is remarkably good.

Figures 10(a)–(d) show the ratios R_{n4} (n = 0–3) as a function of the proton energy. The calculations carried out with the above stabilization probabilities are compared with the present experiment as well as with those from Ben-Itzhak *et al* [13] and Knudsen *et al* [14]. The asymptotic values, at high energies, are associated with the intercept of equations (6)–(9), i.e., single ionization, while the energy dependence below approximately 1 MeV is related to double ionization. The reasonably broad range of velocities in which double ionization contributes, in the proton case, is the main dynamical feature which permits the present method

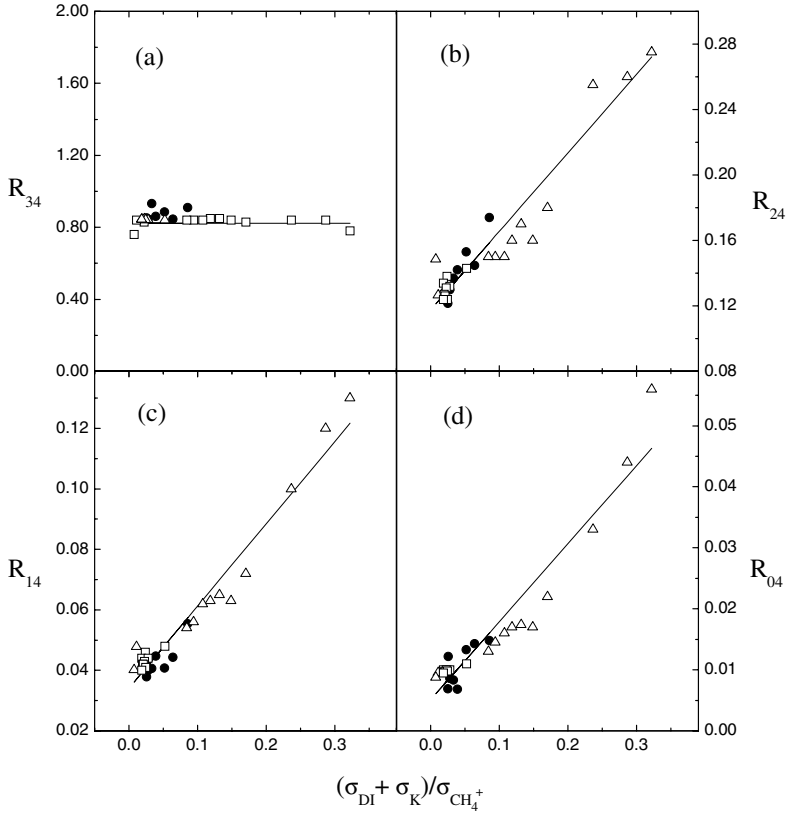

Figure 8. Dissociation ratios R_{n4} ($n = 0$–3) as a function of $(\sigma_{\mathrm{DI}} + \sigma_{\mathrm{K}})/\sigma_{\mathrm{CH_4^+}}$. The symbols are the same as in figure 2.

to be useful. The same does not occur in the electron case. Indeed, the sharp threshold of the R_{n4} ($n = 0$–3) ratios for electron impact makes a similar analysis imprecise due to the weak energy dependence of these ratios after the sharp increase above the threshold. These features are described in the next section.

5. Application: ionization by electrons

At high velocities, the dissociation routes for electrons should be rather similar to those for protons, as the differences in the dynamics of energy transfer for these two particles are small. However, it is possible that these small differences can cause changes in the numerical values of the stabilization probabilities. Processes leading to double ionization, such as shake-off or two-step mechanisms [35, 36], can result in different energy transfers either due to differences in mass or in charge as well as due to the role played by dynamical electron–electron correlation. Indeed, differences between single- and double-ionization cross sections in multielectron targets, by electron and proton impact have been reported by Melo *et al* [37]. The double-ionization yields of Ar induced by electrons and positrons also show clear differences in their dependences on the energy transfer, possibly due to the differences in the trajectory followed by positive and negative particles in close collisions [38]. Three-body electron correlation, which occurs in double ionization by electrons, has been clearly identified

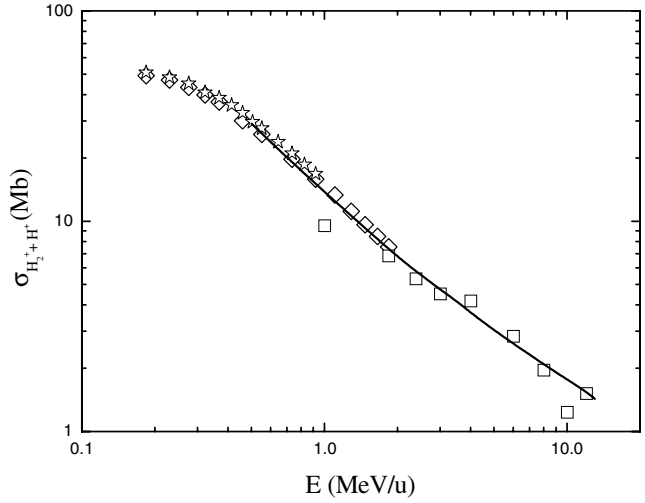

Figure 9. H^+ plus H_2^+ production cross section as a function of projectile energy for proton and electron impact. Protons: □, [13]. Electrons: ☆, [17]; ◇, [18]. Full curve: this work.

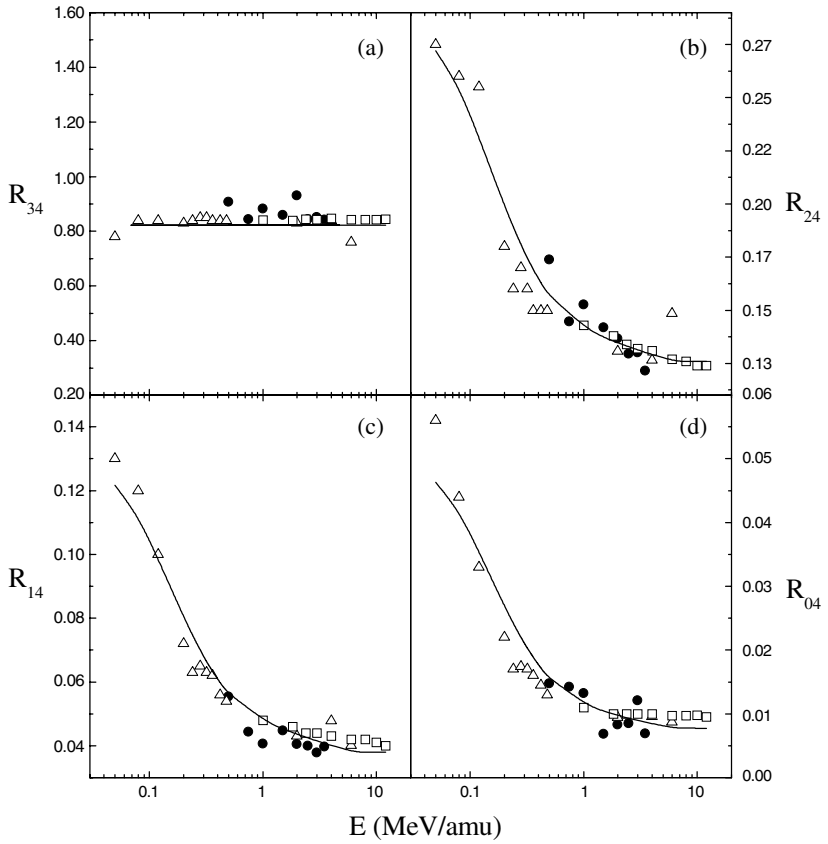

Figure 10. Dissociation ratios R_{n4} ($n = 0$–3) by protons as a function of the proton energy. The symbols are the same as in figure 2. Full curve: this work.

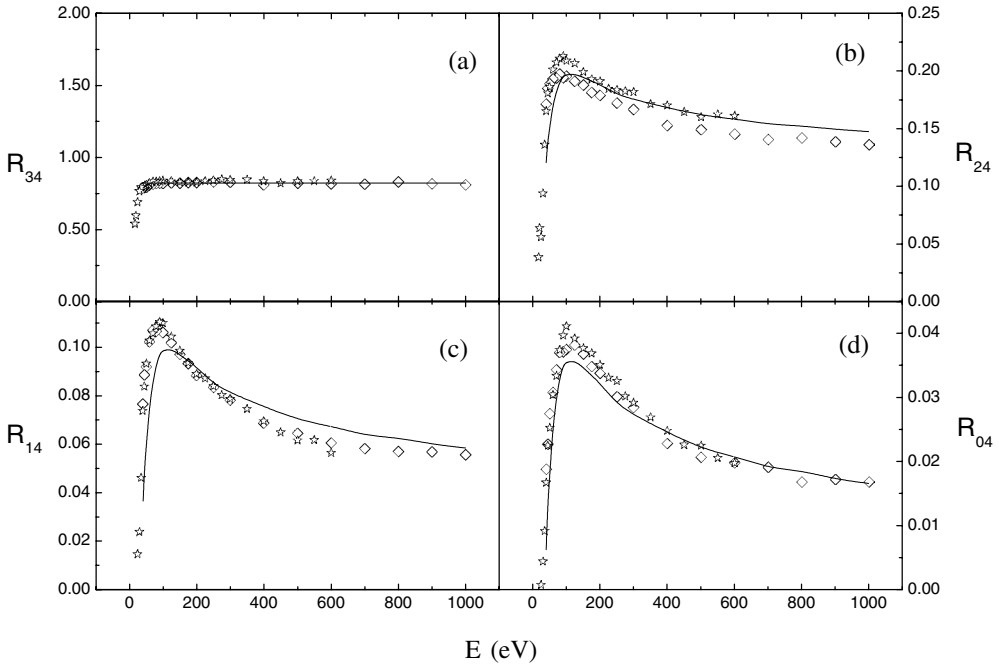

Figure 11. Dissociation ratios R_{n4} ($n = 0$–3) by electrons as a function of the electron energy. ☆, [17]; ♢, [18]. Full curve: this work.

in triple ionization of Ne by highly charged, heavy ion impact [39]. These examples show that the mechanisms leading to energy transfer from charged particles to molecules resulting, in turn, in their various alternatives of dissociation, can be quite complex.

As a reliable calculation for the double ionization of CH_4 by electron impact is not available, we used the experimental measurements of $\sigma_{CH_4^+}$ and $\sigma_{H^+ + H_2^+}$ of Straub *et al* [17] into equations (1) and (11) to determine σ_I and σ_{DI} and, from that, all the ratios R_{n4} ($n = 0$–3). This is shown in figures 11(a)–(d) where, with the exception of p_{2d}, the same stabilization probabilities determined in the proton case are used. We found that a better fit to experiment is obtained if $p_{2d} = 0.40$ instead of $p_{2d} = 0.48$, obtained in the proton case. This 16% difference might be due to different characteristics of the energy transfer of the double-ionization process in the proton and electron cases, as discussed above. The model agrees well with the data from Straub *et al* [17] and Cechan and Vidal [18], both in magnitude and in shape.

6. Conclusions

The consistency of the decay scheme presented in this paper for both proton and electron impact, and over a wide range of projectile velocities provides a reliable organizational picture that can be useful not only in a large variety of applications but also for further studies on CH_4 dissociation by particle impact. Indeed, methane is found in several different environments which can affect its decay due to the change in the population of vibrational levels. Of particular interest is the dependence with temperature which, as shown by Latimer *et al* [22] in the ionization by VUV photons, can change the ratio R_{24} by a factor of 5, if the temperature changes from 300 to 100 K. How the stabilization probabilities depend on the temperature is an open question, but the proposed model can help to address this problem in a clearer way.

Acknowledgments

One of us (ECM) would like to thank M B Shah for fruitful discussions on molecular dissociation. This work was supported in part by the Brazilian agencies CNPq, CAPES, FAPERJ, and MCT (PRONEX), and by the Volkswagen Stiftung (Germany).

References

[1] Cravens T E, Lindgren C J and Levina S A 1998 *Planet. Space Sci.* **46** 1193
[2] Samuelson R E 2003 *Planet. Space Sci.* **51** 127
[3] Lara L M, Banaszkiewics M, Rodrigo R and Lopez-Moreno J J 2002 *Icarus* **158** 191
[4] Johnson R E 1994 *Space Sci. Rev.* **69** 215
[5] Luna H, Michael M, Shah M B, Johnson R E, Latimer C J and McConkey J W 2003 *J. Geophys. Res.* **108** 5033
[6] Zhang W and Catherine Y 1991 *Surf. Coat. Technol.* **47** 69
[7] Masi M, Cavallotti C and Carrà S 1998 *Chem. Eng. Sci.* **22** 3875
[8] Browning R and Gilbody H B 1968 *J. Phys. B: At. Mol. Phys.* **1** 1149
[9] Carré M 1967 *Thesis* University of Lyon
[10] Malhi N B, Ben-Itzhak I, Gray T J, Legg J C, Needham V, Carnes K D and McGuire J H 1987 *J. Chem. Phys.* **87** 6502
[11] Gray T J, Cocke C L and Justiniano E 1980 *Phys. Rev.* A **2** 849
[12] Ben-Itzhak I, Carnes K D, Ginther S G, Johnson D T, Norris P J and Weaver O L 1993 *Phys. Rev.* A **47** 3748
[13] Ben-Itzhak I, Carnes K D, Johnson D T, Norris P J and Weaver O L 1994 *Phys. Rev.* A **49** 881
[14] Knudsen H, Mikkelsen U, Paludan K, Kirsebom K, Möller S P, Uggerhöj E, Slevin J, Charlton M and Morenzoni E 1995 *J. Phys. B: At. Mol. Opt. Phys.* **28** 3569
[15] Poulsen M R, Frandsen N P and Knudsen H 1994 *Hyperfine Interact.* **89** 73
[16] Backx C and Van der Wiel M J 1975 *J. Phys. B: At. Mol. Phys.* **8** 3020
[17] Straub H C, Lin D, Lindsay B G, Smith K A and Stebbings R F 1997 *J. Chem. Phys.* **106** 4430
[18] Cechan T and Vidal C R 1998 *J. Phys. B: At. Mol. Opt. Phys.* **31** 895
[19] Samson J A R, Haddad G N, Masuoka T, Pareek P N and Kilcoyne D A L 1989 *J. Chem. Phys.* **90** 6925
[20] Dutuit O, Aït-Kaci M, Lamaire J and Richard-Viard M 1990 *Phys. Scr.* T **31** 223
[21] Field T A and Eland J H D 1995 *J. Electron Spectrosc. Relat. Phenom.* **73** 209
[22] Latimer C J, Mackie R A, Sands A M, Kouchi N and Dunn K F 1999 *J. Phys. B: At. Mol. Opt. Phys.* **32** 2667
[23] Santos A C, Melo W S, Sant'Anna M M, Sigaud G M and Montenegro E C 2002 *Rev. Sci. Instrum.* **73** 2396
[24] Cavalcanti E G, Sigaud G M, Montenegro E C, Sant'Anna M M and Schmidt-Böcking H 2002 *J. Phys. B: At. Mol. Opt. Phys.* **35** 3937
[25] Khan J M, Potter D L and Worley R D 1965 *Phys. Rev.* A **139** 1735
[26] Yu Y C, McNeir M R, Weathers D L, Duggan J L, Mc Daniel F D and Lapicki G 1991 *Phys. Rev.* A **44** 5702
[27] Gardner R K and Gray T J 1978 *At. Data Nucl. Data Tables* **21** 515
[28] Krause M O 1979 *J. Phys. Chem. Ref. Data* **8** 307
[29] Furuya K, Ishikawa K and Ogawa T 2000 *Chem. Phys. Lett.* **319** 335
[30] Mathur D 1981 *Chem. Phys. Lett.* **81** 115
[31] Dujardin G, Winkoum D and Leach S 1985 *Phys. Rev.* A **31** 3027
[32] Siegbahn P E M 1982 *Chem. Phys.* **66** 443
[33] Sant'Anna M M, Montenegro E C and McGuire J H 1998 *Phys. Rev.* A **58** 2148 and references therein
[34] Kirchner T, Lüdde H J and Dreizler R M 1999 *Phys. Rev.* A **61** 012705
[35] McGuire J H, Berrah N, Bartlett R J, Samson J A R, Tanis J A, Cocke C L and Schlachter A S 1995 *J. Phys. B: At. Mol. Opt. Phys.* **28** 913
[36] McGuire J H 1997 *Electron Correlation Dynamics in Atomic Collisions* (Cambridge: Cambridge University Press)
[37] Melo W S, Santos A C F, Sant'Anna M M, Sigaud G M and Montenegro E C 2002 *J. Phys. B: At. Mol. Opt. Phys.* **35** L187
[38] Santos A C F, Hasan A, Yates T and DuBois R D 2003 *Phys. Rev.* A **67** 052708
[39] Schulz M, Moshammer R, Schmitt W, Kollmus H, Mann R, Hagmann S, Olson R E and Ullrich J 2000 *Phys. Rev.* A **61** 022703